Rigaku

X-ray Diffraction & Elemental Analysis

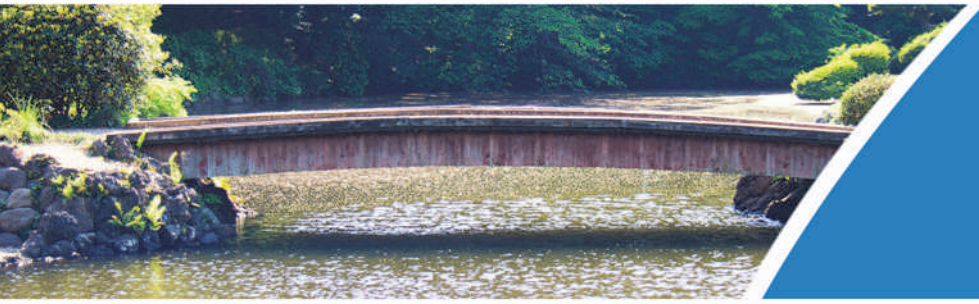

橋 THE BRIDGE

MATERIALS ANALYSIS eNEWSLETTER
AUGUST 2014, ISSUE 14

Welcome

Although scientists and people involved in technology are often portrayed as anti-social, nothing could be further from the truth. All one has to do is to attend a technical conference and watch life-long relationships being formed between people who share an interest in discovery and understanding. While the internet has dropped many barriers for the flow of information, it will never replace the importance of developing human relationships in scientific endeavors as a positive mechanism for cross-pollination of ideas. While travel budgets continue to be hard to obtain, it is important to continue interacting with other like-minded people in order to stay fresh in your perspective and to challenge your mental growth.

Enjoy the newsletter.

BRIDGE 橋

A bridge is often used to symbolize a connection or link between two places, and thus we felt The Bridge would be the perfect name for our eNewsletter, as we hope that it will act as a vehicle for the transmission of ideas and information between Rigaku and interested readers around the world.

And a bridge is a two-way structure, a concept that we will keep in mind as we not only provide information about Rigaku, but also report on interesting research and the associated laboratories around the world, publish technical book reviews that might help our readers in their work, and highlight general news topics that are of interest to many people involved in materials analysis.

Photo by Paul Swepston

Featured Rigaku Journal Article

The latest X-ray diffraction techniques for advanced research and development in lithium-ion battery materials

Akira Kishi, Application laboratory, Rigaku Corporation

Lithium-ion battery technology continues to improve and will be an important energy technology for the future. This paper describes recent expectations for X-ray diffractometers in research and development of lithium-ion batteries. It also introduces measurement methods that respond to those expectations.

Click here for full article

The XtaLAB PRO Series

Rigaku has developed a new series of single crystal diffractometers that address a wide range of sample types, from small molecules to MOFs to biological macromolecules. The key component that is common for this series of diffractometers is the use of an HPAD (hybrid pixel array detector) detector, a technology that produces an almost perfect detector and greatly expands the capabilities of a single crystal diffractometer in terms of speed of data acquisition and more accurate measurement of weak data. The standard detector in the XtaLAB PRO series is the PILATUS 200 (Figure 1), a detector that is well proven in the field and based on the same technology adopted by synchrotron beamlines around the world. The outstanding characteristics of these detectors ensure that every XtaLAB PRO diffractometer will perform to produce the best data possible for the X-ray source selected.

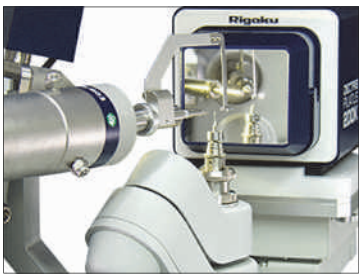

Figure 1. The PILATUS 200 HPAD detector

Why the HPAD outperforms other detectors

There are three characteristics of the HPAD detector that make it especially good for the measurement of single crystal diffraction data. First, the readout speed of the detector is so fast that the diffractometer can be run in true shutterless mode. The shutter is opened at the beginning of a scan and the scan axis moves continuously until the scan is finished. Images are constantly being readout during the scan and since the readout time is insignificant they can be treated the same way that single images are normally handled. Shutterless data collection mode can lead to significantly faster data acquisition.

The second characteristic of the HPAD detector that makes shutterless data collection a routine technique is the high dynamic range of the detector. This means that rescans due to intense reflections are not necessary. With a CCD detector, the shutter is opened and closed with each image and you have to wait as the image is read out. If there is an overload (due to the restricted dynamic range) then a rescan has to occur. In addition to

the speed improvement, shutterless data collection eliminates errors that are associated with the opening and closing of shutters as well as the ramping up and ramping down of scan axes.

The third important characteristic of the HPAD detector is the fact that the noise level is essentially zero (no detector is perfect and so it is not correct to call it a noiseless detector, but the HPAD is the closest thing to a noiseless detector available today). A detector with extremely low noise is important because it means that you can measure weak reflections more accurately since backgrounds are as low as possible. Any crystal will have a combination of relatively weak and strong reflections but crystals that most benefit from the accurate measurement of weak reflections are crystals that scatter poorly. With an HPAD detector, the low noise characteristic means that you can expose a crystal for significantly longer periods of time than either a CCD or a CMOS based detector. There is no significant build up of noise with the HPAD detector and you can measure diffraction from poorly diffracting crystals that would be swamped with electronic noise in other types of detectors.

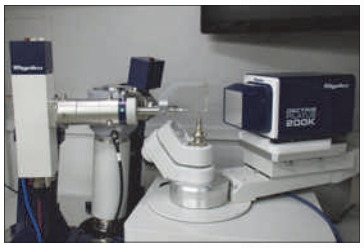

Figure 2. The standard configuration of the XtaLAB PRO series includes a PILATUS 200 detector, a kappa goniometer, a Cu microfocus sealed tube source (MicroMax-003) and a 3 kW Mo sealed tube source

X-ray source configurations

While the HPAD detector is the common element of the XtaLAB PRO series, the selection of X-ray sources is quite diverse and allows one to select an X-ray source configuration based on the radiation type or types as well as the level of flux desired.

The standard configuration for the XtaLAB PRO (Figure 2) includes a Cu MicroMax™-003 microfocus sealed tube source and a 3 kW Mo standard sealed tube source with a SHINE (curved graphite monochromator) optic. The selection of a microfocus Cu source and a standard focus Mo source is based on the difference in efficiency between Cu and Mo radiations when coupling micro focal spots with multilater optics. Figure 3 shows the relative flux through a 100 µm aperture at the crystal position for both a standard sealed tube Cu source with graphite monochromator and a microfocus Cu X-ray source with a multilayer optic. The approximately 12-fold improvement in flux at the sample makes the use of the Cu microfocus X-ray source an easy decision.

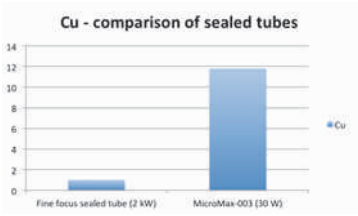

Figure 3. Relative flux through a 100 µm aperture at the crystal position for sealed tube Cu sources

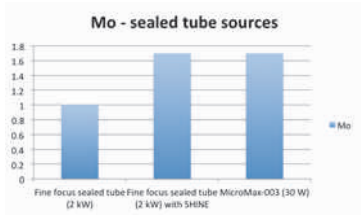

Figure 4. Relative flux through a 100 µm aperture at the crystal position for sealed tube Mo sources

Figure 4 shows the relative flux through a 100 µm aperture at the crystal position for a standard sealed tube Mo source with graphite monochromator, a standard sealed tube Mo source with a curved graphite monochromator (SHINE optic) and a microfocus Mo X-ray source with a multilayer optic. It is easy to see that the standard Mo source with the SHINE optic produces equivalent X-ray flux at the sample as the microfocus Mo source. However, when crystals are larger than 100 µm the standard sealed tube X-ray source is better because the beam is larger. The collimator can easily be changed to ensure that the X-ray beam is at least as large as the crystal. With microfocus X-ray sources, the X-ray beams are roughly 100 µm in diameter and for large crystals, the sample will not be fully bathed in the X-ray beam. *Continued on next page*

Featured EDXRF Application Note

Pt, Pd, Rh in recycled automotive catalysts

Applied Rigaku Technologies

Used catalytic converters are collected and recycled in order to reclaim the precious metals Pt, Rh and Pd. In this application note, the measurement of Pt, Rh and Pd in recycled automotive catalytic converters is demonstrated using data from a NEX QC benchtop spectrometer and utilizing a Fundamental Parameters (FP) approach and pre-installed starter Matching Library for data alanysis.

Click here to see full application note

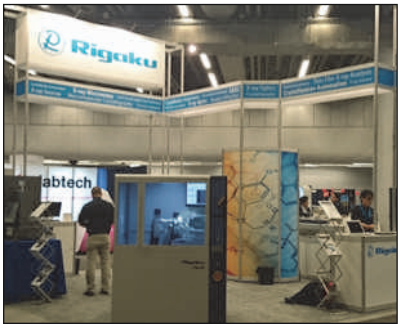

Conferences and Workshops

Join Rigaku at future meetings

Earlier this month, Rigaku exhibited at the IUCr Congress in Montreal. Shown above is the Rigaku booth, where the new XtaLAB PRO single crystal diffractometer was introduced.

Rigaku will be sponsoring, attending or exhibiting at the following conferences and trade shows:

JASIS 2014
Makuhari Messe, Japan
September 3 – 5

18th International Microscopy Congress
Prague, Czech Republic
September 7 – 12

Canadian Mineral Analysts
Saskatchewan, Canada
August 5 – 12

See the complete list

Beyond the standard configuration of the XtaLAB PRO, it is possible to increase the flux at the sample significantly by utilizing a rotating anode based X-ray source and Rigaku offers a number of models and configurations to choose from.

MicroMax-007 HF

FR-X

The MicroMax-007 HF is a microfocus rotating anode generator and the most popular rotating anode source utilized for single crystal analysis around the world. It is available in both a single wavelength configuration and a unique double wavelength configuration. In the double wavelength configurations (Mo/Cu or Cu/Cr), the wavelength to be used can be selected automatically.

For even more flux at the sample, the FR-X microfocus rotating anode generator is available and is the most powerful rotating anode X-ray source for single crystal analysis available today.

These two rotating anode sources are well proven in the field and offer a low-maintenance regimen compared to rotating anodes of the past. While the ongoing maintenance of a rotating anode generator is more than that of a sealed tube generator, the flux at the sample is significantly higher and allows researchers to measure samples that could only previously be measured at a synchrotron.

Figures 5 and 6 shows the relative flux through a 100 µm aperture at the crystal position for a standard sealed tube source, a microfocus sealed tube source, the MicroMax-007 HF, and the FR-X for Cu and Mo radiation respectively.

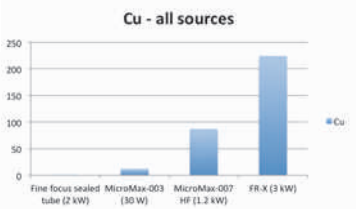

Figure 5. Relative flux through a 100 µm aperture for all Cu sources

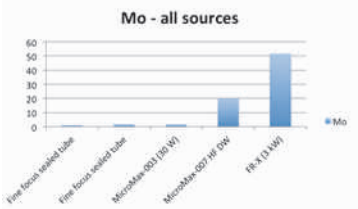

Figure 6. Relative flux through a 100 µm aperture for all Mo sources

For Cu radiation, the 7 and 19 fold increases in flux for the MicroMax-007 HF and FR-X respectively compared to the MicroMax-003 (microfocus sealed tube) is a clear indication of the performance improvements that are possible when using rotating anode based X-ray sources. It is even more significant for Mo radiation, where 12 and 30 fold improvements can be gained from the MicroMax 007 HF and FR-X respectively compared to a Mo sealed tube source with a SHINE optic or a Mo microfocus sealed tube source.

A work environment designed for research

The XtaLAB PRO series is housed in a newly developed enclosure (Figures 7 and 8) that was designed to improve the workflow of mounting air-sensitive and temperature sensitive samples. There is space inside the XtaLAB PRO enclosure for a microscope and a dewar. No matter what type of samples you are working with, the ability to identify and mount crystals in the proximity of the diffractometer can be a true time saver. In the case of air-sensitive and temperature-sensitive crystals, having close proximity of the mount-

ing station to the goniometer can mean the difference between a crystal that diffracts and a crystal that dies.

Figure 7. The front of the XtaLAB PRO enclosure can be fully opened for easy access

Figure 8. There is enough space inside of the XtaLAB PRO enclosure to place critical experimental equipment.

Click here for more information on the XtaLAB PRO

Lab in the Spotlight

IUCr-UNESCO OpenLab Colombia-Venezuela

A Rigaku sponsored IUCr-UNESCO OpenLab will be held at the end of October at Laboratorio de Rayos X, Parque Tecnológico Guatiguará (Piedecuesta), Universidad Industrial de Santander, Bucaramanga, Colombia. Participation in this OpenLab is limited to 30 students and applications will be accepted on a first-come/first-served basis. The organizers are José Antonio Henao (UIS-Colombia), Graciela Díaz de Delgado (ULA-Venezuela), Miguel Delgado (ULA-Venezuela), and Akihiko Iwata (Rigaku Corporation).

Event Name:
Rigaku OpenLab Colombia-Venezuela

Start Date:
October 27

End Date:
October 31

Duration:
5 days

Location:
Laboratorio de Rayos X, PTG, Piedecuesta, Colombia

Contact:
Prof. José Antonio Henao (Colombia)
jahenao@uis.edu.co, jahenao@gmail.com

Prof. Miguel Delgado (Venezuela)
migueld@ula.ve

Website:
http://www.rigaku.com/events/openlab

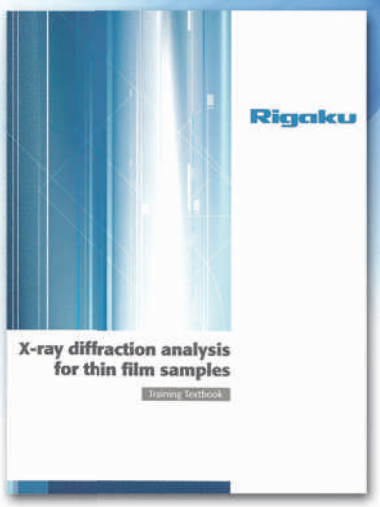

Thin Film Training Textbook

Overview of the principles of X-ray reflectivity (Part 8)

This month we finish the chapter on X-ray reflectivity by looking at the analysis of the magnetic film on glass that was in last month's excerpt, to demonstrate a general analysis of reflectivity. A summary of the reflectivity chapter is also included. Next month we start to cover high resolution X-ray diffraction.

Click here for Part 8

Scientific Book Review

Stuff Matters: Exploring the Marvelous Materials that Shape our Man-Made World
By Mark Miodownik

Houghton Mifflin Harcourt Publishing, New York, 272 pp, ISBN: 978-0544236042

Mark Miodownik's book, *Stuff Matters*, is a delightful approach to the history and the science of modern materials by a materials scientist. His structure and approach for the book is unique—unlike anything I've encountered yet in popular science nonfiction.

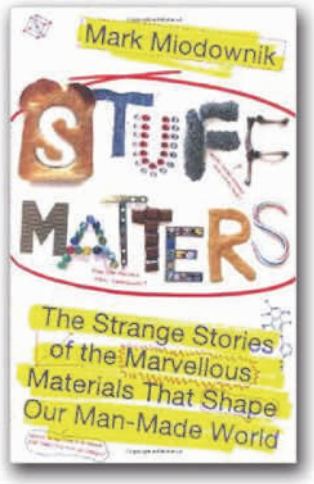

Miodownik starts with a black-and-white photograph of himself sitting at a table on the roof of his flat. Each chapter begins with a reproduction of that photograph, but with an arrow pointing to a different object and a label describing the object's composition. He offers a brief history of each material, laced with a personal anecdote or two, and often accompanied by a hand-drawn illustration of its molecular composition.

Perhaps the most entertaining chapter is that on chocolate. A self-professed "chocaholic," Miodownik's passion for the popular food is evident. Given the fame of Swiss chocolate, I had always thought that the solid bar form was invented in Switzerland, but it was, in fact, an English firm called Fry and Sons that first produced "eating chocolate." However, this chocolate, which had thirty percent sugar added, was too bitter. The Swiss were the first to use milk to combat this bitterness, essentially inventing what we now know as milk chocolate. They used the powdered milk recently introduced by Nestlé, a company that was attempting to give a localized commodity with virtually no shelf-life a transportable quality and a longer shelf-life.

It was quite fortunate for the Swiss that Nestlé was pioneering powdered milk at the same time that Fry's introduced their too-bitter eating chocolate. Adding regular non-powdered milk to the chocolate would have been disastrous. Chocolate powder is hydrophilic, and will absorb water; however, because fat and water do not dissolve in each other (fat is hydrophobic), the chocolate powder would eject its fat coating, making the resulting liquid lumpy and generally regarded as unappetizing. One can only imagine the differences in our modern world if powdered milk had never been developed.

Miodownik's passion for the subject (of) matter as a materials scientist is evident in his prose, and makes the book a quick and easy read. There is very little technical jargon that might impede the enjoyment of the book by someone not trained in materials science, or even the sciences in general. Miodownik is a man who loves what he does, and sees his work in the world around him. This book is a testament to his desire to inspire excitement for materials science in those around him as well.

Jeanette S. Ferrara,
Princeton, Class of 2015

WDXRF Application Note

Ultra-low (ppb) quantitative analysis using UltraCarry method for river water standard JAC0032

Water investigation for contaminants that could be harmful to humans and surrounding flora and fauna is not typically done by XRF due to the very low levels of detection required for this analysis. Government regulations are in place to monitor harmful substances in water. Lead (Pb), chromium (Cr), arsenic (As), and selenium (Se) are some of the more important analytes of interest because of the potentially adverse effects these trace metals have on the brain and reproductive systems in human and animal alike, as well as the mutagenic changes they can cause in crop and plant life.

Figure 1

The UltraCarry preparation method uses a filter paper to concentrate an aqueous liquid sample on a specially designed absorbent pad that is mounted on a Mylar film, which is stretched across a rigid plastic disk. This unusual sample holder (as seen in Figure 1) allows the Rigaku ZSX® Primus II WDXRF spectrometer to do a standard water type analysis in only a few minutes and attain values at the PPB level, which rival its competitive ICP analysis method for sensitivity- while offering a drastically reduced preparation set-up time.

The specially designed UltraCarry method was used in the following analysis of river water standard JAC0032 (River Water standard) for ultra low ppb levels of Pb, Cr, As and Se. Because the standard contains such low concentration levels it was pre-concentrated from 50 mL to 500 µL. Spectral scans of the hazardous analytes of interest can be for Pb, Se, As, and Cr, respectively.

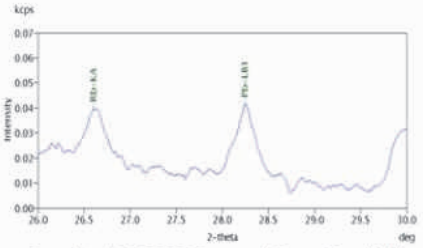

Standard JAC0032-Spectral Scan 10 ppb Pb

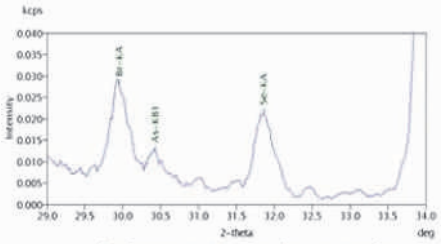

Standard JAC0032-Spectral Scan 5 ppb Se

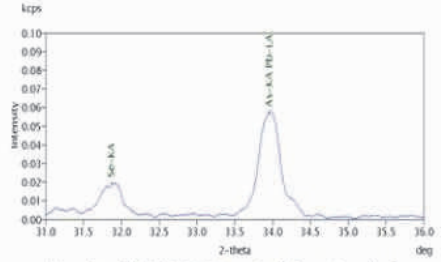

Standard JAC0032-Spectral Scan 5 ppb As

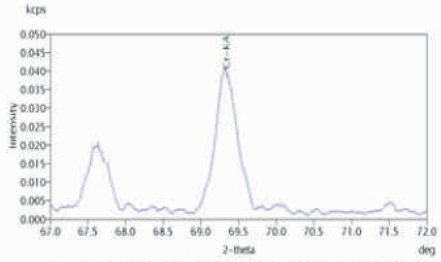

Standard JAC0032-Spectral Scan 10 ppb Cr

Quantitative calibrations were created using typical AA standard solutions dried on the UltraCarry. The lower limits of detection for each element are shown in Table 1.

Element	Pb	Cr	Cd	As	Se
LLD (ppb)	40	45	109	12	13

Table 1

500 microliters of the pre-concentrated river water sample (1/100 concentration) was then dripped and dried on the UltraCarry and run under a vacuum atmosphere. The resulting values of the test sample were then recalculated back to an "as received" basis producing the final results shown in Table 2.

Element	Pb	Cr	Cd	As	Se
Quantitative results (ppb)	13.7	11.8	1.6	4.0	9.7
Standard value (ppb)	9.9	10.1	1.0	5.2	5.5

Table 2

ZSX Primus II features an innovative optics-above configuration. Never again worry about a contaminated beam path or down time due to sample chamber maintenance. The optics-above geometry eliminates cleaning worries and increases up time. Read more…

Material Analysis in the News

August 1, 2014. NASA announced that its next rover to Mars, in 2020, will carry seven special instruments to conduct an unprecedented study of the red planet. Scientists picked the seven instruments from 58 proposals that NASA received in January from researchers and engineers around the world. Mars 2020 rover will also carry an X-ray fluorescence spectrometer called "Planetary Instrument for X-ray Lithochemistry" to collect high-resolution images for details about chemical elements on the planet's surface.

August 8, 2014. NASA's Curiosity rover marks two Earth years on Mars this month, and Planetary Science Institute researchers are actively pursuing new knowledge of our neighboring planet. The sedimentary rock samples tested were collected at Yellowknife Bay in Gale Crater on Mars. The rover's CheMin X-Ray Diffraction and Fluorescence (CheMin XRD/XRF) instrument analyzed the samples. The *in situ* X-ray diffraction results reveal the presence of smectite, a type of clay mineral typical of soils and sediments that have not been deeply buried, heated, or otherwise altered.

August 12, 2014. Lasers can be used to identify chemical powders, such as explosives or fertilizers, from hundreds of meters away by exploiting Raman spectroscopy in conjunction with a phenomenon called random lasing. This latest work was supported in part by the US Air Force and conducted at its research facilities in San Antonio, Texas.

August 14, 2014. Researchers studying the contents of a capsule returned to Earth in 2006, at the conclusion of the Stardust spacecraft's primary mission, believe that they have found seven remarkable specks on its collection panels. Scientists subjected these interstellar dust particles to X-ray diffraction studies.

August 16, 2014. Scientists say they can now identify mercury-containing skin creams and intervene much faster than before, speeding up the process and making a safer environment for consumers. The research, using the total reflection X-ray fluorescence (TXRF) technique, was presented at the National Meeting & Exposition of the American Chemical Society (ACS) in San Francisco.

August 16, 2014. University of Tennessee, Knoxville, associate professor Claudia Rawn has been named a 2014 ASM International Fellow, earning one of the highest honors attainable in her field. She is director of the Center for Materials Processing and a member of both iBME, the Institute for Biomedical Engineering, and JIAM, the Joint Institute for Advanced Materials. The award stems from her work using in situ X-ray and neutron diffraction to study a variety of novel energy materials from superconductors to gas hydrates. She and other members of this year's class will be formally inducted at an Oct. 14 meeting in Pittsburgh.

August 18, 2014. Maria Varela, a researcher at Oak Ridge National Laboratory, has received the Microscopy Society of America's Burton Medal for early career scientists. Varela's research experience includes thin-film growth, transport properties, and structural characterization by X-ray diffraction and electron microscopy. She specializes in aberration corrected scanning transmission electron microscopy and atomic resolution energy loss spectroscopy.

August 19, 2014. An international team of researchers claims to have proven the stability of silicene. The research demonstrated for the first time that thick, multilayer silicene films can be stable in air for at least 24 hours. While 24 hours doesn't seem like a long time, it should give researchers a window of opportunity to perform more tests on the material to reveal its capabilities.

August 19, 2014. The National Science Foundation has awarded Indiana University- Purdue University Indianapolis a $374,989 grant to purchase an advanced X-ray diffraction system, through the Major Research Instrumentation Program. The XRD system, which will be housed in and maintained by the Integrated Nanosystems Development Institute in collaboration with the Department of Earth Science, enhances IUPUI's shared instrumentation profile and supports faculty and students across many schools and departments by providing capabilities for a range of interdisciplinary scientific discovery and workforce training.

August 19, 2014. Global process spectroscopy market expected to reach USD 1.2 billion in 2019. North America was the largest contributor to global process spectroscopy market in 2012. Asia Pacific region is expected to be the fastest growing market for process spectroscopy during the forecast period with a CAGR of 8.7% from 2013 to 2019. The rapid growth of process spectroscopy technologies in pharmaceutical and food and agriculture industries in Asia Pacific region, particularly in countries like China, Japan and India is driving the growth of process spectroscopy market in Asia Pacific region.

The Adventures of Captain Nano

IT'S JUST A JUMP TO THE LEFT...

Can Captain Nano free himself from the nanoparticle?

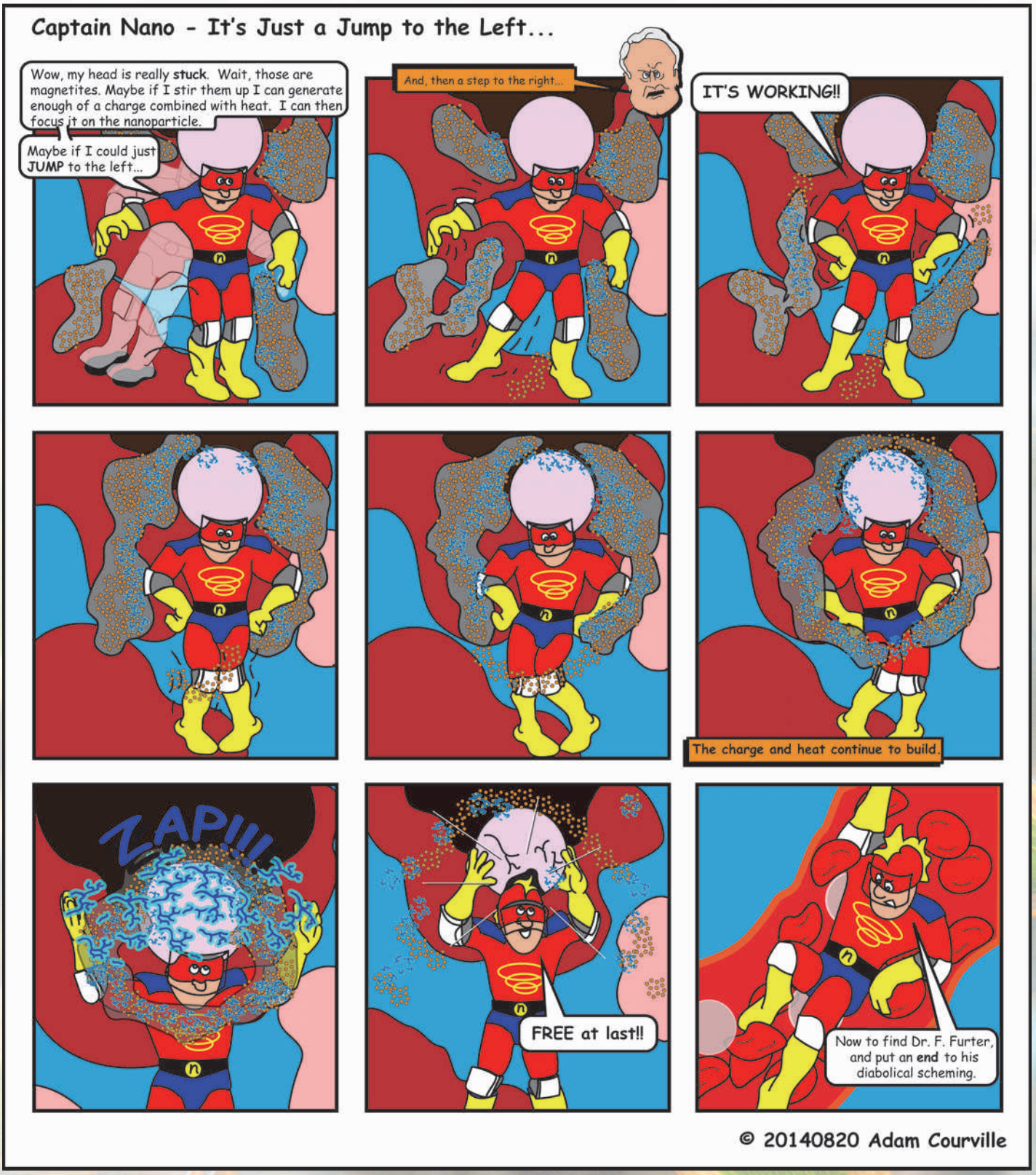

Recent Scientific Papers of Interest

Environmental nuclear-geophysical ore monitoring in mines of Corporation Kazakhmys PLC. Yefimenko, Sergei; Yefimenko, Olga; Makarov, Dmitriy. Journal of Environmental Science & Health, Part A: Toxic/Hazardous Substances & Environmental Engineering. Aug2014, Vol. 49 Issue 10, p1163-1170. 8p. DOI: 10.1080/10934529.2014.897530.

Cycled Thermomechanical Failure in 808-nm High-Power AlGaAs/GaAs Laser Diode Bars. Qiao, Yanbin; Feng, Shiwei; Zhang, Gongchang; Xiong, Cong; Zhu, Hui; Guo, Chunsheng. IEEE Transactions on Electron Devices. Aug2014, Vol. 61 Issue 8, p2854-2858. 5p. DOI: 10.1109/TED.2014.2331333.

Performance Evaluation of Currently Used Portable X ray Fluorescence Instruments for Measuring the Lead Content of Paint in Field Samples. Muller, Yan; Favreau, Philippe; Kohler, Marcel. Journal of Occupational & Environmental Hygiene. Aug2014, Vol. 11 Issue 8, p528-537. 10p. DOI: 10.1080/15459624.2014.880788.

Strain state, film and surface morphology of epitaxial topological insulator Bi_2Se_3 films on Si(111). Klein, C.; Vyshnepolsky, M.; Kompch, A.; Klasing, F.; Hanisch-Blicharski, A.; Winterer, M.; Hoegen, M. Horn-von. Thin Solid Films. Aug2014, Vol. 564, p241-245. 5p. DOI: 10.1016/j.tsf.2014.04.024.

Structural and paramagnetic behavior of spinel $NiCr_2O_4$ nanoparticles synthesized by thermal treatment method: Effect of calcination temperature. Bakar, Syuhada Abu; Mat Yunus, W. Mahmood; Soltani, Nayereh; Saion, Elias; Bahrami, Afarin. Solid State Communications. Aug2014, Vol. 192, p15-19. 5p. DOI: 10.1016/j.ssc.2014.05.002

Controlling of crystallite orientation for poly(ethylene oxide) thin films with cellulose single nano-fibers. Fukuya, Miki Noda; Kazunobu Senoo; Kotera, Masaru; Yoshimoto, Mamoru; Osami Sakata. Polymer. Aug2014, Vol. 55 Issue 16, p4401-4404. 4p. DOI: 10.1016/j.polymer.2014.06.004.

Influence of remelting on oxidation behaviour and hardness of $Sm_{56}Al_{26}Co_{18}$ amorphous alloy. Corrosion Engineering, Science & Technology. Aug2014, Vol. 49 Issue 5, p357-362. 6p. DOI: 10.1179/1743278213Y.0000000145.

The 400°C Isothermal Section of the La-Co-Mg Ternary System. Negri, S.; Solokha, P.; Saccone, A. Journal of Phase Equilibria & Diffusion. Aug2014, Vol. 35 Issue 4, p377-383. 7p. DOI: 10.1007/s11669-014-0290-1.

Stress relaxation due to ultrasonic impact treatment on multi-pass welds. Science & Technology of Welding & Joining. Aug2014, Vol. 19 Issue 6, p505-513. 9p. DOI: 10.1179/1362171814Y.0000000219.

Phase change materials for thermal energy storage. Pielichowska, Kinga; Pielichowski, Krzysztof. Progress in Materials Science. Aug2014, Vol. 65, p67-123. 57p. DOI: 10.1016/j.pmatsci.2014.03.005.

Possibilities of micro X-ray fluorescence spectrometry of solutions with preconcentration. Bolotokov, A.; Gruzdeva, A.; Khamizov, R.; Kumakhov, M. Journal of Analytical Chemistry. Aug2014, Vol. 69 Issue 8, p728-734. 7p. DOI: 10.1134/S1061934814060033.

Materials Characteristics of Roman and Arabic Mortars and Stuccoes from the *Patio De Banderas* in the Real Alcazar of Seville (Spain). Garofano, I.; Robador, M. D.; Duran, A. Archaeometry. Aug2014, Vol. 56 Issue 4, p541-561. 21p. DOI: 10.1111/arcm.12041.

The low-temperature form of calcium gold stannide, CaAuSn. Lin, Qisheng; Corbett, John D. Acta Crystallographica: Section C, Structural Chemistry. Aug2014, Vol. 70 Issue 8, p773-775. 3p. DOI: 10.1107/S205322961401612X.

Electrosynthesis of Co/PPy nanocomposites for ORR electrocatalysis: a study based on quasi-in situ X-ray absorption, fluorescence and in situ Raman spectroscopy. Bocchetta, Patrizia; Gianoncelli, Alessandra; Abyaneh, Majid Kazemian; Kiskinova, Maya; Amati, Matteo; Gregoratti, Luca; Jezeršek, David; Mele, Claudio; Bozzini, Benedetto. Electrochimica Acta. Aug2014, Vol. 137, p535-545. 11p. DOI: 10.1016/j.electacta.2014.05.098.

Effect of Silicate Content on the Properties of Alkali-Activated Blast Furnace Slag Paste. Qureshi, Mohammed; Ghosh, Somnath. Arabian Journal for Science & Engineering (Springer Science & Business Media B.V.). Aug2014, Vol. 39 Issue 8, p5905-5916. 12p. DOI: 10.1007/s13369-014-1172-x.

Effect of Thickness and Deposition Rate on the Structural and Magnetic Properties of Evaporated Fe/Al Thin Films. Mebarki, M.; Layadi, A.; Kerkache, L.; Benabbas, A.; Tiercelin, N.; Preobrazhensky, V.; Pernod, P. Journal of Superconductivity & Novel Magnetism. Aug2014, Vol. 27 Issue 8, p1951-1957. 7p. DOI: 10.1007/s10948-014-2552-x.

Detection of macrosegregation in a large metallic specimen using XRF. Ironmaking & Steelmaking. Aug2014, Vol. 41 Issue 7, p493-499. 7p. DOI: 10.1179/1743281213Y.0000000144.

Evolution of clay mineral assemblages in the Tinguiririca geothermal field, Andean Cordillera of central Chile: an XRD and HRTEM-AEM study. Vázquez, M.; Nieto, F.; Morata, D.; Droguett, B.; Carrillo-Rosua, F. J.; Morales, S. Journal of Volcanology & Geothermal Research. Aug2014, Vol. 282, p43-59. 17p. DOI: 10.1016/j.jvolgeores.2014.05.022.

Assessing the quality of metallurgical coke by Raman spectroscopy. Rantitsch, Gerd; Bhattacharyya, Anrin; Schenk, Johannes; Lünsdorf, Nils Keno. International Journal of Coal Geology. Aug2014, Vol. 130, p1-7. 7p. DOI: 10.1016/j.coal.2014.05.005.

The contribution of Raman spectroscopy to the analytical quality control of cytotoxic drugs in a hospital environment: Eliminating the exposure risks for staff members and their work environment. Bourget, Philippe; Amin, Alexandre; Vidal, Fabrice; Merlette, Christophe; Troude, Pénélope; Baillet-Guffroy, Arlette. International Journal of Pharmaceutics. Aug2014, Vol. 470 Issue 1/2, p70-76. 7p. DOI: 10.1016/j.ijpharm.2014.04.064.

Raman spectroscopy applied to the horizontal methods ISO 6579:2002 to identify *Salmonella* spp. in the food industry. Assaf, A.; Cordella, C.; Thouand, G. Analytical & Bioanalytical Chemistry. Aug2014, Vol. 406 Issue 20, p4899-4910. 12p. DOI: 10.1007/s00216-014-7909-2.

Mechanical behavior study of microdevice and nanomaterials by Raman spectroscopy: a review. Qiu, Wei; Kang, Yi-Lan. Chinese Science Bulletin. Aug2014, Vol. 59 Issue 23, p2811-2824. 14p. DOI: 10.1007/s11434-014-0401-8.

Objective geological logging using portable XRF geochemical multi-element data at Plutonic Gold Mine, Marymia Inlier, Western Australia. Michael F. Gazley, Chelsea M. Tutta, Louise A. Fisherb, Aaron R. Lathama, Guillaume Duclauxc, Mike D. Taylora, Samuel J. de Beera. Journal of Geochemical Exploration. Volume 143, August 2014, Pages 74–83. DOI: 10.1016/j.gexplo.2014.03.019.

Advanced X-ray Spectrometric Techniques for Characterization of Nuclear Materials: An overview of recent laboratory activities. N.L. Misra. Spectrochimica Acta Part B: Atomic Spectroscopy. Available online 13 August 2014. DOI: 10.1016/j.sab.2014.07.021.

Laboratory Total Reflection X-Ray Fluorescence Analysis for Low Concentration Samples. D. Hampai, S.B. Dabagov, C. Polese, A. Liedl, G. Cappuccio. Spectrochimica Acta Part B: Atomic Spectroscopy. Available online 13 August 2014. DOI: 10.1016/j.sab.2014.07.020.

Spatial Convolution of a Stress Field Analyzed by X-Ray Diffraction. Kahloun, C., Badji, R., Queyreau, S., Franciosi, P., & Bacroix, B. Advanced Materials Research. Aug2014, Vol. 996, pp. 169-174. DOI: 10.4028/www.scientific.net/AMR.996.169.

Combining XRD with Hole-Drilling Method in Residual Stress Gradient Analysis of Laser Hardened C45 Steel. Kolařík, K., Pala, Z., Ganev, N., & Fojtik, F. Advanced Materials Research. Aug2014, Vol. 996, pp. 277-282. DOI: 10.4028/www.scientific.net/AMR.996.277.

Validation of a numerical model used to predict phase distribution and residual stress in ferritic steel weldments. Hamelin, Cory J.; Muránsky, Ondrej; Smith, Michael C.; Holden, Thomas M.; Luzin, Vladimir; Bendeich, Philip J.; Edwards, Lyndon. Acta Materialia. Aug2014, Vol. 75, p1-19. 19p. DOI: 10.1016/j.actamat.2014.04.045.

Numerical analysis of retained residual stresses in C(T) specimen extracted from a multi-pass austenitic weld and their effect on crack growth. Muránsky, O.; Smith, M. C.; Bendeich, P. J.; Hosseinzadeh, F.; Edwards, L. Engineering Fracture Mechanics. Aug2014, Vol. 126, p40-53. 14p. DOI: 10.1016/j.engfracmech.2014.04.008.

EDXRF Application Note
Pt, Pd, Rh in Recycled Automotive Catalysts
#1370 Rev2

SCOPE
The measurement of Pt, Rh and Pd in recycled automotive catalytic converters is demonstrated using Fundamental Parameters (FP) approach and pre-installed starter Matching Library.

BACKGROUND
Used catalytic converters are collected and recycled in order to reclaim the precious metals Pt, Rh and Pd. Typically, the entire honeycomb core is removed and ground into a powder. Once in powder form, the precious metal catalysts can be extracted, or the powder can be sold to a refiner.

The honeycomb core, also called the monolith, is typically ceramic, containing combinations of the elements Al, Si, Fe, Zn, Sr, Zr, Ba, La and Ce. Some cores can be made of a stainless steel honeycomb and so would contain higher Fe and other metals. Catalyst material may also be high in Pb content, in regions where leaded gasoline is still used. Because all of these elements can occur at various levels, Rigaku's software offers quick direct analysis and easy use for crafting individual methods, as desired.

INSTRUMENTATION

Model:	Rigaku NEX QC
X-ray tube:	50 kV 4 W Ag-anode
Detector:	Semiconductor
Sample Type:	Powders
Film:	Mylar
Environment:	Air
Analysis Time:	200 seconds
Sample Ring:	Single Position
Optional:	6-position 32mm Autosampler
	Single Position Sample Spinner
	Manual Sample press

Applied Rigaku Technologies, Inc. • 9825 Spectrum Drive, Bldg. 4, Suite 475 • Austin, TX 78717 USA
www.RigakuEDXRF.com • info@RigakuEDXRF.com • (+1) 512-225-1796

SAMPLE PREPARATION

Samples are ground and measured as dry, homogeneous powder. It is not necessary to make hydraulically pressed pellets. A ball mill or mixer mill may be used to take the material down to a powder. For analysis, approximately 5g of powder is poured into an XRF sample cup and simply tapped a few times on a hard surface to compact the sample to ensure consistent sample presentation, or use the Manual Sample Press for consistent compaction.

FUNDAMENTAL PARAMETERS and MATCHING LIBRARY

For screening purposes Fundamental Parameters (FP) is used which calculates concentration based on theory. A factory installed Matching Library for mixed, homogenized materials is included with the analyzer, using twelve samples that have been fire assayed, including two certified NIST standards. FP uses the library information to more closely match XRF with fire assay results, thus providing a more accurate model of the real matrix.

The software is simple and intuitive, allowing the user to expand on the starter Matching Library, or design new Matching Libraries to suite various specific converter materials. Empirical calibrations can also be crafted in order to ensure the optimum accuracy for a specific material type.

The factory starter Matching Library covers the following ranges for Pt, Pd and Rh

.

Element	Concentration Range (ppm)
Pt	400-6230
Pd	260-6445
Rh	0-365

TYPICAL RESULTS

To demonstrate the results using the starter Matching Library, two unknown field samples that had associated fire assay numbers were measured that were not included in the Matching Library.

Sample 9 Units: ppm			
Element	Fire Assay Value	NEX QC Result	% Relative Difference
Pt	392	438	11.7%
Pd	509	526	3.3%
Rh	94	83	11.7%

Sample 12 Units: ppm			
Element	Fire Assay Value	NEX QC Result	% Relative Difference
Pt	1336	1452	8.7%
Pd	922	931	1.0%
Rh	331	329	0.6%

In general, when using a library of similar materials typical accuracy is approximately 10-15% relative or better. Accuracy can be improved by augmenting the Matching Library with additional samples and using longer analysis count times. Highest accuracy is achieved by building separate methods for each specific material. The simple and intuitive software of the NEX QC allows the user to easily create new Matching Libraries and methods.

RECOVERY & PRECISION

The European reference standard was selected to demonstrate repeatability (precision) and is considered a check sample, not part of the factory Matching Library. ERM-EB504E was measured in static position for ten repeat measurements. Typical performance results are shown below.

Sample ID: ERM-EB504E Units: ppm			
Component	Certified Value	NEX QC Average Value	Standard Deviation
Pt	1777	1789	27
Pd	279	266	5
Rh	338	325	6

CONCLUSION

Determination of the precious metals content of recovered catalytic converter cores is critical to accessing the valuations needed in this specialized business within the automotive recycling stream. Intuitive software allows the user to easily expand libraries or create new libraries. Thus, the Rigaku NEX QC and simple yet versatile software provides an easy-to-use and valuable tool for the catalytic converter recycling industry.

Rigaku

X-ray Diffraction Analysis for Thin Film Samples

Training Textbook

Click below to see previously published sections

4.6 Example of Measurement

Fig. 4.6.2 shows an example of a measurement for a superlattice multilayer film. This profile corresponds to the superlattice multilayer film shown in Fig. 4.6.2. The profile shows the superlattice peaks corresponding to the thickness of the period of the layers.

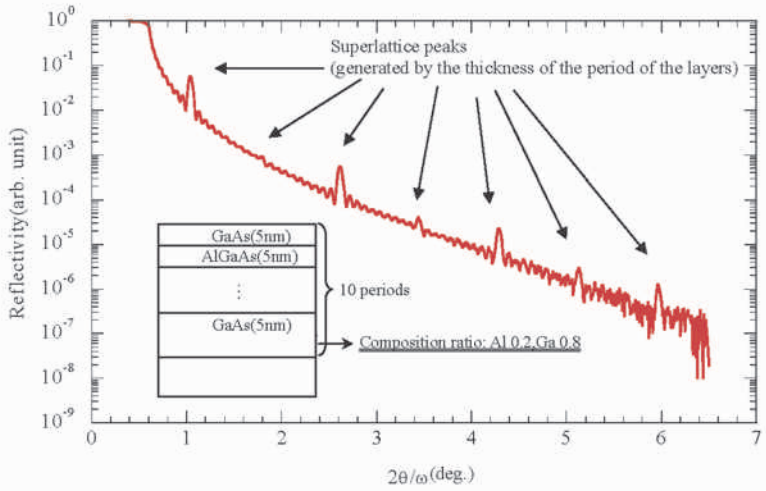

Figure 4.6.2. Example of reflectivity profile for superlattice multilayer film

4.7 Examples of Analysis

Here we take the example of the magnetic film shown in Fig. 4.6.1 to demonstrate a general analysis of reflectivity.

The analysis is performed as indicated in the flowchart shown in Fig. 4.7.1.

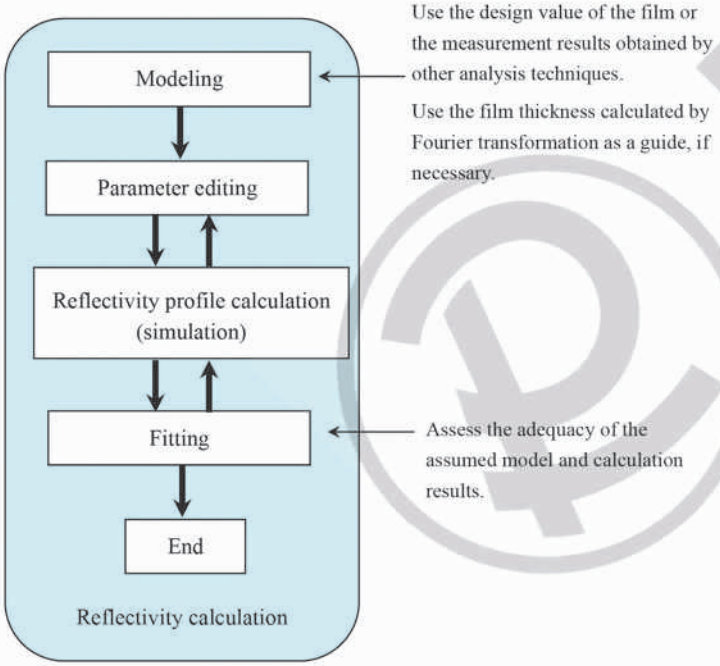

Figure 4.7.1. Procedural flow of reflectivity analysis

Fig. 4.7.2 shows the multilayer film model for the sample analyzed.

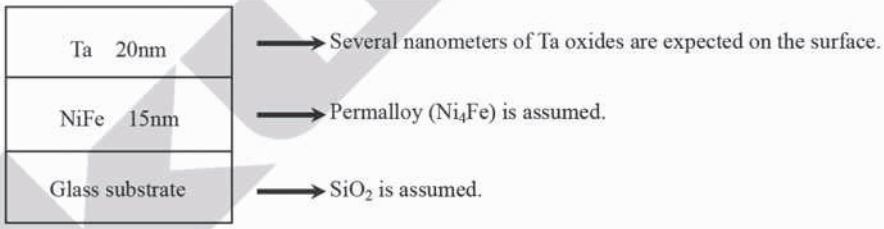

Figure 4.7.2. Multilayer model of magnetic film

Load the measurement data.

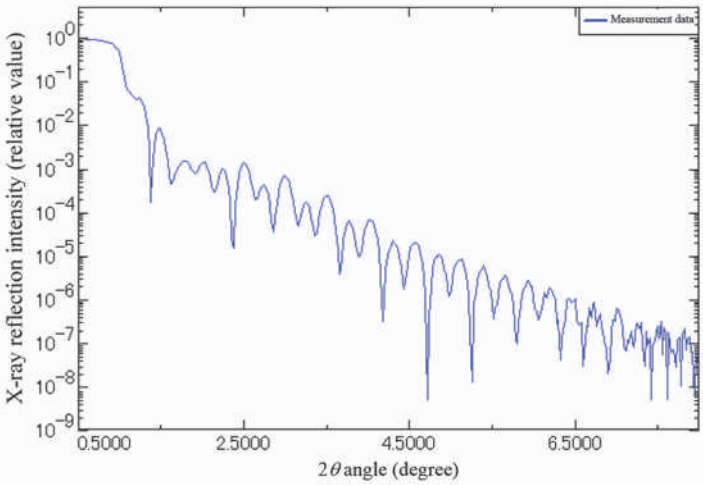

Figure 4.7.3. Measurement data

Set the model and input the thickness of each layer. The results of simulations with these parameters are as follows:

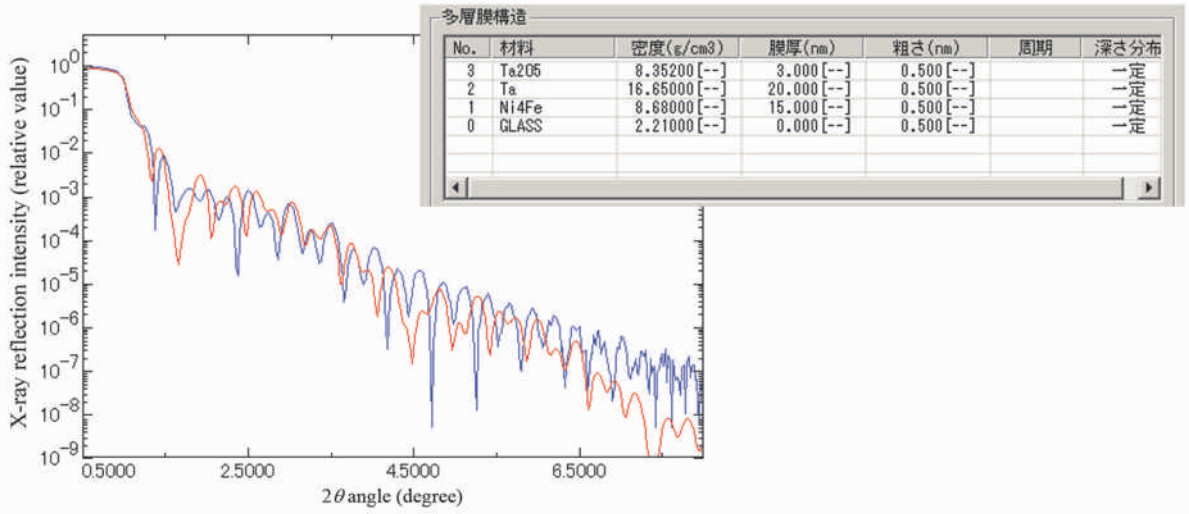

Figure 4.7.4. Results of simulation

4.7 Examples of Analysis

Change the values of the parameters to bring the simulation results closer to the measured profile. Here, we reduce the thickness of the Ta.

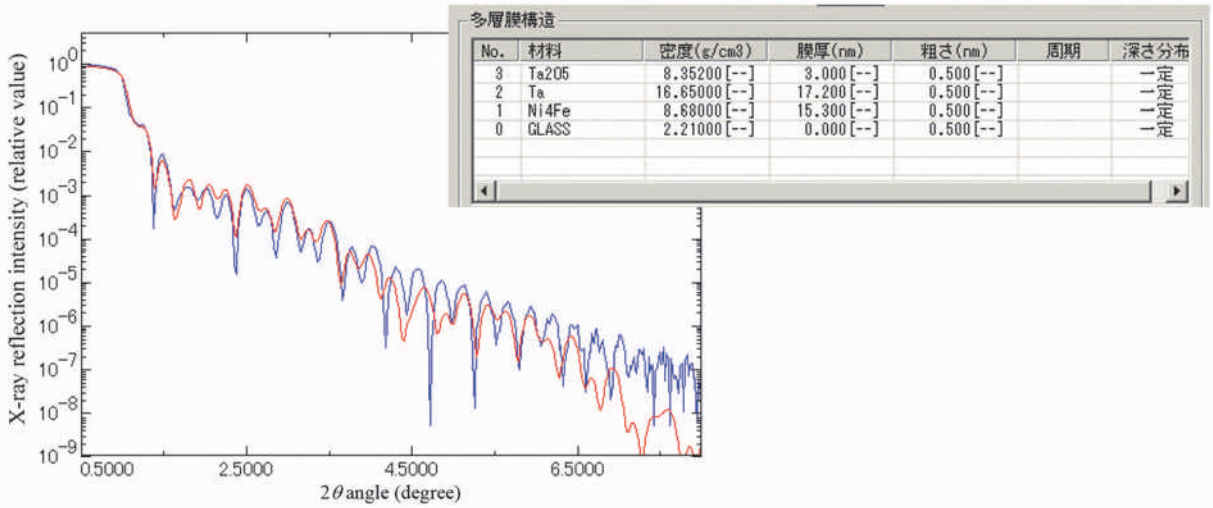

Figure 4.7.5. Results of simulation (Second trial)

The measured profile and the simulation results are now in rough agreement. Now, perform fitting.

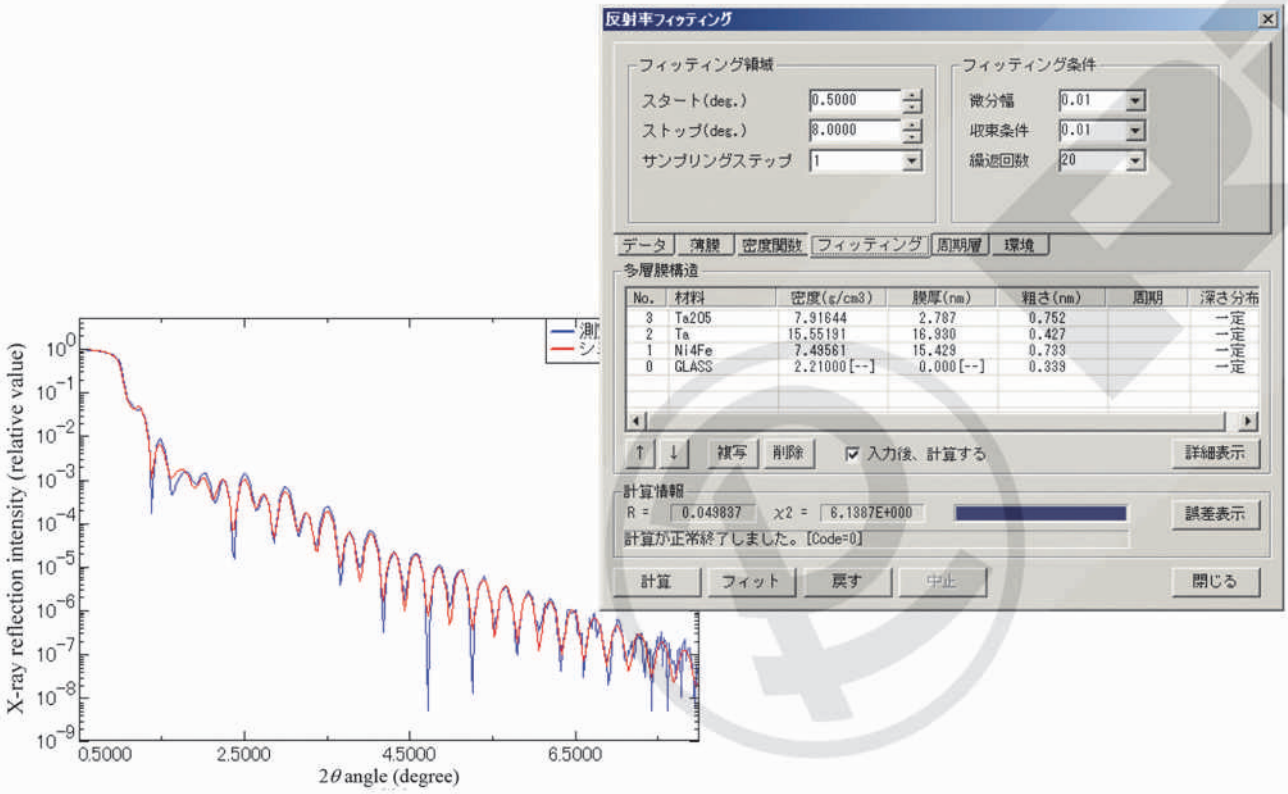

Figure 4.7.6. Results of fitting

In this analysis, the fitting is successful, and the measured profile and calculation result are in near-perfect agreement. The R value displayed below the parameter box in Fig. 4.7.6 indicates the degree of agreement in the method of least squares. As this value approaches zero, the measured profile and the calculation result are in closer agreement. (Use this only as a guide; use the profile to judge whether the measurement and calculations agree.)

In this example, the fitting is successful in the first trial. For fitting to succeed in this way, the simulation result must be as close as possible to the measured profile.

Even when the fitting is successful, there is no guarantee that the calculated value is correct in absolute terms. We need to investigate to confirm whether the calculated solution is adequate.

If the measured profile and the simulation result do not agree, the model assumed may be wrong. In such cases, the model needs to be reconsidered.

4.8 Summary

(1) Features of X-ray reflectivity method

1. The sample must be sufficiently flat and smooth.
   (Surface or interface roughness must be on the order of several nanometers or less.)
2. The method can be applied to polycrystalline and amorphous materials.
3. The method is extremely sensitive to surface states.
4. The method is independent of crystal orientation or strain.
5. The method is insensitive to changes in composition.
6. The method can be used to evaluate film thickness of up to approximately 1,000 nm.
   It is not suited to use with thicker films.

(2) Information provided by X-ray reflectivity profile

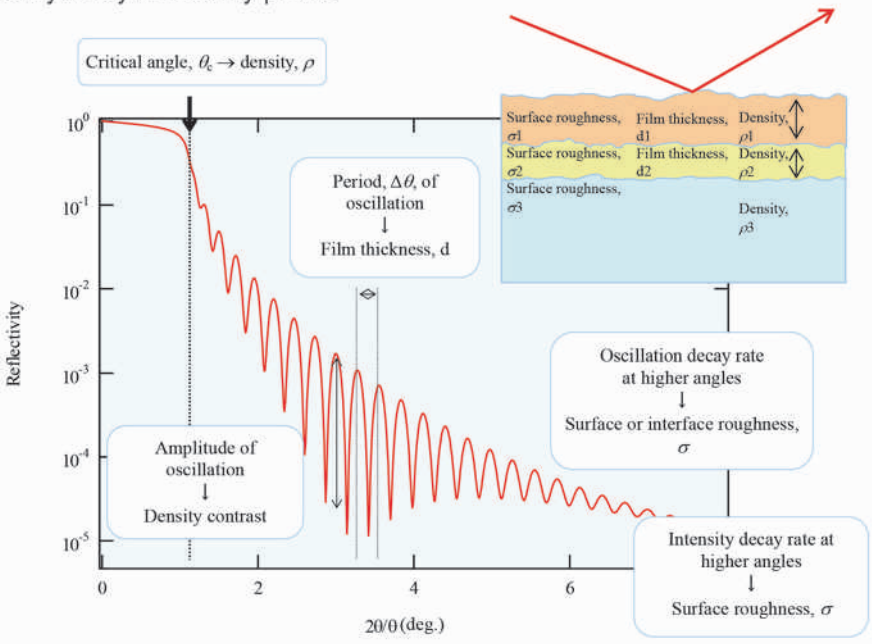

4.8 Summary

(3) Analysis method

1. Method giving film thickness from the incident angle dependence of the oscillation period.
2. Method giving film thickness via Fourier transformation.
3. Method giving film thickness, density, and surface or interface roughness by fitting.

Methods 2 and 3 are now practical under most conditions.

The latest X-ray diffraction techniques for advanced research and development in lithium-ion battery materials

Akira Kishi*

1. Introduction

The materials used in the manufacture of lithium-ion batteries include positive electrode materials, negative electrode materials, electrolytes, separators, binders (for positive and negative electrodes), and cladding materials (for battery housings). Research and development on these materials is active and ongoing.

This paper describes recent expectations for X-ray diffractometers in research and development activities that seek to improve the performance of such materials. It also introduces measurement methods that respond to those expectations.

2. Use of *in situ* cells to analyze changes in crystal structure during charging and discharging

It is recognized that controlling charging and discharging conditions extends the service life of lithium-ion batteries. This control requires more than observations of electrode structures in the fully charged/discharged state; it requires real-time measurements of the relationship between the states of charge/discharge and the electrode structures using in situ cells. The 2011 Spring issue of Rigaku Journal introduced the results of *in situ* X-ray diffraction measurements of changes in the crystal structure of olivine-type positive electrode $LiFePO_4$ (provided by Tatsuya Nakamura, Professor, Graduate School of Engineering, University of Hyogo) using lithium-battery cells[1]. In this experiment, when the state of charge (SOC) was 0%, the material was $LiFePO_4$. However, as SOC increased, X-ray diffraction peaks generated by $FePO_4$ began to appear. At 100% SOC, X-ray diffraction patterns indicated a near-complete $FePO_4$ phase after a coexistence state of two phases. Professor Nakamura and Yashiro (of Rigaku Corporation) *et al.* recently showed that a slight peak shift occurs at 20% SOC relative to 0% SOC, and that lattice constants decrease by around 0.05%. However, virtually no change in lattice constants occurs from that state to 60% SOC. These findings were presented in the conference held by the Electrochemical Society (U.S.A.) in October 2011[2]. As this example suggests, we believe detailed analyses of changes in crystal structure during charging and discharging will become increasingly important in controlling charge/discharge states.

3. Observations of trace quantities of coexisting compounds

Research and development efforts currently target various compounds for use as positive and negative electrode materials. Since positive electrode materials are multi-element metal oxides, compounds differing slightly in composition or crystal structure may be mixed in during synthesis, or slight changes may occur in the crystal structure or composition of the material during repeated charges/discharges. In addition, trace amounts of compound may be deliberately added to improve the material performance. Conventionally, X-ray diffractometry has been used for qualitative and quantitative analysis of trace amounts of coexisting compounds and for analysis of polymorphic compounds having identical chemical composition but different crystal structure. This method is widely used for both inorganic and organic materials. We expect similar demand to grow in the field of lithium-ion battery materials.

3.1. Measurements using D/teX Ultra, high-speed one-dimensional detector

The features and characteristics of the D/teX Ultra high-speed one-dimensional detector have been described in Rigaku Journal[3]. This detector offers roughly 100 times the detection sensitivity of scintillation counters. It is ideally suited to measurements of materials for lithium-ion batteries, because this detector offers high energy resolution that reduces the effects of fluorescent X-rays from Co, Fe, or other materials found in the positive electrode material of the lithium-ion battery. Figure 1 compares measuring results of $CoLiO_2$ removed from a coin cell battery charged and discharged 100 times, using a scintillation counter and the D/teX Ultra.

3.2. Measurements using Kα1 optics and D/teX Ultra

When a Cu target is used as an X-ray source, the following three K-series X-rays with neighboring wavelengths are included: Kβ1 1.392 Å, Kα1 1.541 Å, and Kα2 1.544 Å. With the most common X-ray diffraction measurement method, a nickel filter is used to remove peaks by Kβ X-rays. However, this also reduces the intensity of the sample's other diffraction peaks.

To offset this drawback, the Kα1 optic system is used to extract only Kα1 X-rays. Top level researchers in the field of lithium-ion battery who visit the Rigaku

* Application Laboratory, Rigaku Corporation.

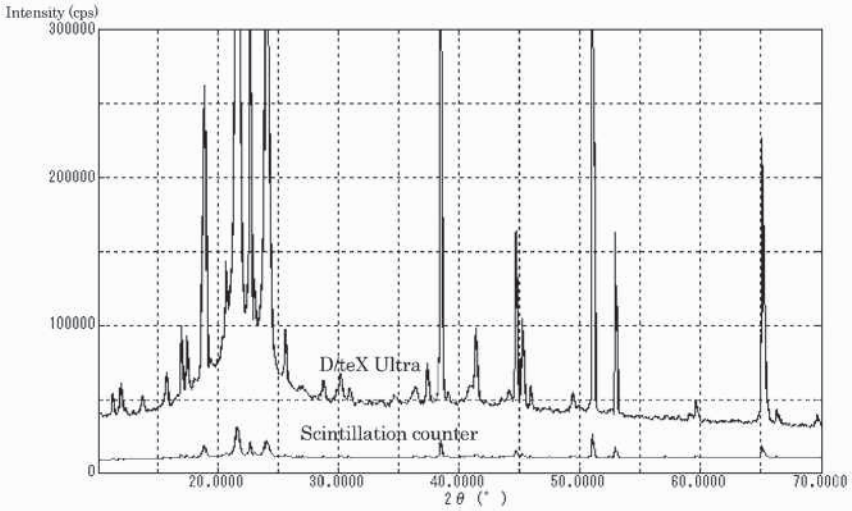

Fig. 1. Comparison of results of $LiCoO_2$ measurements.

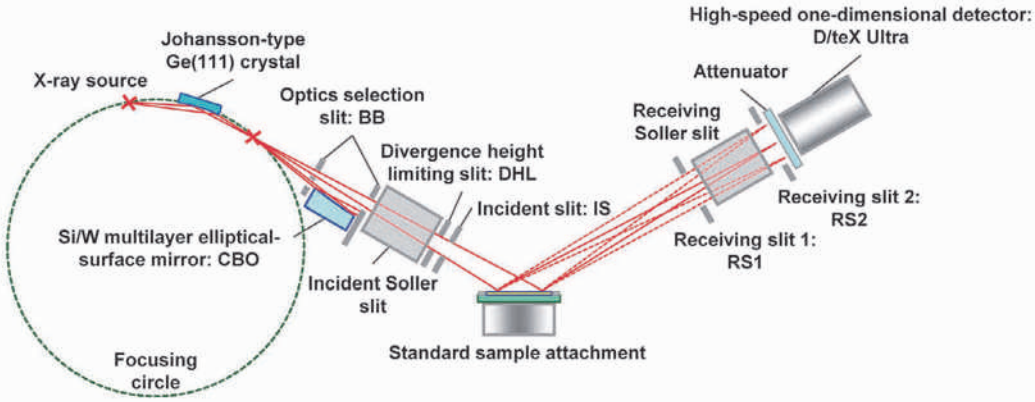

Fig. 2. Schematic of SmartLab with Kα1 optics and D/teX Ultra.

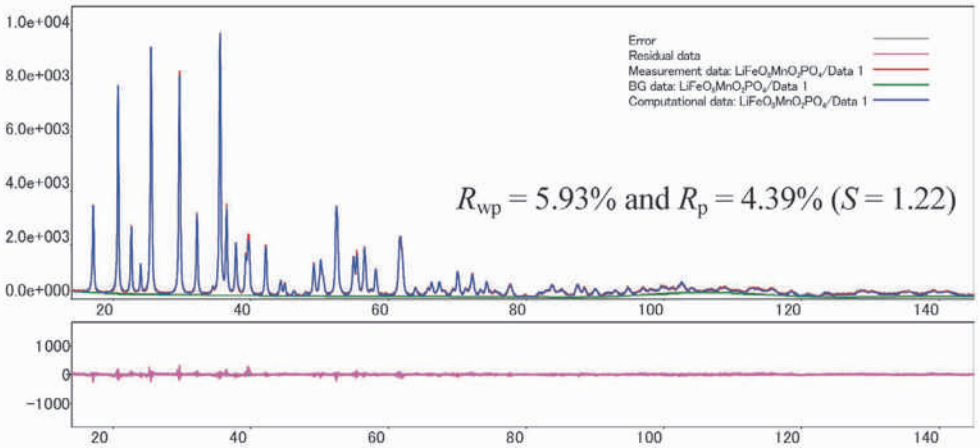

Fig. 3. Results of measurement and analysis.

laboratory often show great interest in the following two newest Rigaku systems. These systems allow to measure infinitesimal impurities in positive electrode materials:

1. The combination of Rigaku's SmartLab Automated Multipurpose X-ray Diffractometer, the Kα1 optics, and the D/teX Ultra,
2. The combination of the Kα optics (Kα1 and Kα2 with intensity ratio of 2 : 1), monochromator, and the D/teX Ultra.

Figure 2 shows a schematic of the SmartLab combined with the Kα1 optics and D/teX Ultra.

To date, measurements of infinitesimal compounds have been very hard to perform without a synchrotron radiation facility like SPring-8. However, the capacity to

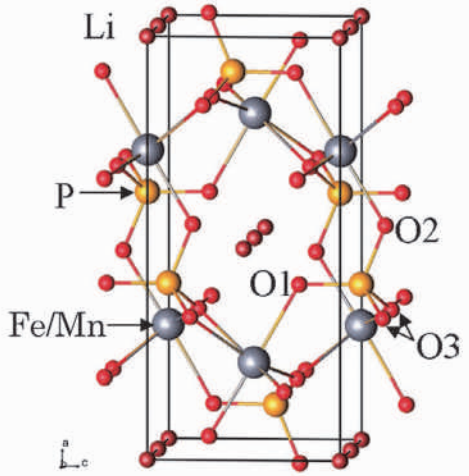

Fig. 4. Crystal structure obtained.

measure minute peaks against background noise in ordinary laboratory settings is expected to advance studies of the positive and negative effects of trace coexisting compounds.

4. Structure analysis of the positive electrode materials of lithium-ion battery based on powder X-ray diffraction data

In the field of lithium-ion battery materials, researchers have expressed more interest in analyzing crystal structures based on powder X-ray diffraction data. Introduced below is an example of an structure analysis of $LiFe_{0.8}Mn_{0.2}PO_4$, an FeMn olivine-type positive electrode material offering excellent thermal stability and safety (sample courtesy of Nobuya Machida, Professor of Department of Chemistry of Functional Molecules, Konan University).

A baked at 550°C sample was measured using the Ultima IV Protectus general-purpose X-ray diffractometer. The results obtained are given in Fig. 3, Fig. 4, Table 1, and Table 2.

Using this method, the relationship between fine structure of various battery materials and their performance will be easily verified in ordinal laboratories.

Table 1. Crystallographic data.

Chemical formula	$LiFe_{0.8}Mn_{0.2}PO_4$
Space group	*Pnma*
a(Å)	10.3463(5)
b(Å)	6.0219(3)
c(Å)	4.7046(2)
Z	4
$D_x(gcm^{-3})$	3.57

Table 2. Structural parameters.

Label	Occupancy	Fractional coordinates			Temperature factor
		x	*y*	*z*	*B* (Å^2)
Fe/Mn	0.8/0.2*	0.28189(5)	1/4	0.0253(8)	0.58(4)
P	1	0.0947(1)	1/4	0.5831(2)	0.56(3)
O1	1	0.0962(3)	1/4	0.2603(5)	0.36(6)
O2	1	0.4558(3)	1/4	0.7922(4)	0.50(6)
O3	1	0.3348(2)	0.5495(3)	0.2163(3)	0.33(4)
Li	1**	0	0	0	1.1(2)

* The ratio of Fe to Mn was fixed (due to the nearby atomic scattering factor.)

** We attempted to obtain the precise occupancy of Li, but since the value was 1.00(1), we set the ratio to 1.

References

(1) *The Rigaku Journal (English version)*, **27** (2011), No. 32–35.

(2) T. Nakamura, S. Masuda, Y. Yamada, H. Takahara and W. Yashiro: 220th ECS Meeting and Electrochemical Energy Summit (2011), Session B6, Abstract No. 647.

(3) *The Rigaku Journal (English version)*, **24** (2008), No. 30–32.

Rigaku

THE BRIDGE

MATERIALS ANALYSIS eNEWSLETTER

AUGUST 2014, ISSUE 14